ACS OMEGA

http://pubs.acs.org/journal/acsodf

Article

Exploration of SARS-CoV-2 Mpro Noncovalent Natural Inhibitors Using Structure-Based Approaches

Cuong Quoc Duong and Phuong Thuy Viet Nguyen*

Cite This: *ACS Omega* 2023, 8, 6679−6688

Read Online

ACCESS | Metrics & More | Article Recommendations | Supporting Information

ABSTRACT: With the emergence of antibody-evasive omicron subvariants (BA.2.12.1, BA.4, and BA.5), which can compromise the efficacy of vaccination, it is of utmost importance to widen the finite therapeutic options for COVID-19. Although more than 600 co-crystal complexes of Mpro with inhibitors have been revealed, utilizing them to search for novel Mpro inhibitors remains limited. Although there were two major groups of Mpro inhibitors, covalent and noncovalent inhibitors, noncovalent inhibitors were our main focus due to the safety concerns with their covalent counterparts. Hence, this study aimed to explore Mpro noncovalent inhibition ability of phytochemicals extracted from Vietnamese herbals by combining multiple structure-based approaches. By closely inspecting 223 complexes of Mpro with noncovalent inhibitors, a 3D-pharmacophore model representing typical chemical features of Mpro noncovalent inhibitors was generated with good validation scores (sensitivity = 92.11%, specificity = 90.42%, accuracy = 90.65%, and goodness-of-hit score = 0.61). Afterward, the pharmacophore model was applied to explore the potential Mpro inhibitors from our in-house Vietnamese phytochemical database, revealing 18 substances, 5 of which were *in vitro* assayed. The remaining 13 substances were then examined by induced-fit molecular docking, revealing 12 suitable compounds. A machine-learning activity prediction model was developed to rank the hit, suggesting nigracin and calycosin-7-*O*-*β*-glucopyranoside as promising Mpro natural noncovalent inhibitors.

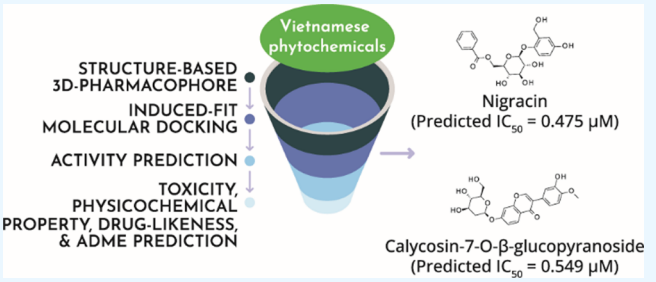

1. INTRODUCTION

Since the declaration of COVID-19 as a global pandemic by the WHO in 2019,[1] the vast spread of SARS-CoV-2 has caused more than 600 million confirmed cases and millions of deaths, becoming one of the most detrimental global health crises in modern history.[2] Although vaccination has been approved worldwide, treatments for SARS-CoV-2 remain limited.[3,4] Moreover, with the surge of SARS-CoV-2 omicron subvariants,[5] especially the antibody-evasive ones (BA.2.12.1, BA.4, and BA.5),[6] the efficacy of COVID-19 vaccines and therapeutic monoclonals is compromised.[6] Thus, there is an utmost need for the discovery of efficient therapeutic agents against SARS-CoV-2. Several targets that play essential roles in the viral replication are being studied in the search for SARS-CoV-2 inhibitors, including the main protease (Mpro).[7] Due to its high conservation among related viruses, Mpro has become an appealing target for developing SARS-CoV-2 antiviral drugs.[7]

SARS-CoV-2 Mpro inhibitors can be divided into covalent inhibitors (such as N3, GC376) and noncovalent inhibitors (such as X77, ML188).[8] The covalent inhibitors block the binding site by forming a covalent bond with Mpro, usually with Cys145 in the catalytic dyad His41-Cys145.[7] By contrast, the noncovalent ones can inhibit Mpro without using any form of covalent bond.[7] However, despite the merits of covalent inhibitors and their resurgence recently, their safety aspects, including the potential side-effects from off-targeting and prolonged effects, have always been a distaste for the revelation of novel drugs.[9,10] Though there are a handful of highly selective covalent Mpro inhibitors (such as compound 18) that do not inhibit human cysteine protease (like cathepsin B and L),[11] many potent covalent inhibitors with enzymatic inhibition and cellular antiviral activity (including GC376, boceprevir, calpain inhibitors II, and XII) are not as selective as their noncovalent counterparts (such as 23R and ML188).[8] Moreover, in terms of inhibiting Mpro, the potency of irreversible covalent Mpro inhibitors was less reliable due to the limitation of conventional IC_{50} measurements (having different incubation times will lead to different IC_{50} values).[7] Hence, noncovalent inhibitors remain the focus of this research since they can act alone or provide starting points for developing safer covalent inhibitors.

One of the most fascinating aspects in the search for SARS-CoV-2 inhibitors is the sheer amount of identified

Received: November 11, 2022
Accepted: January 23, 2023
Published: February 6, 2023

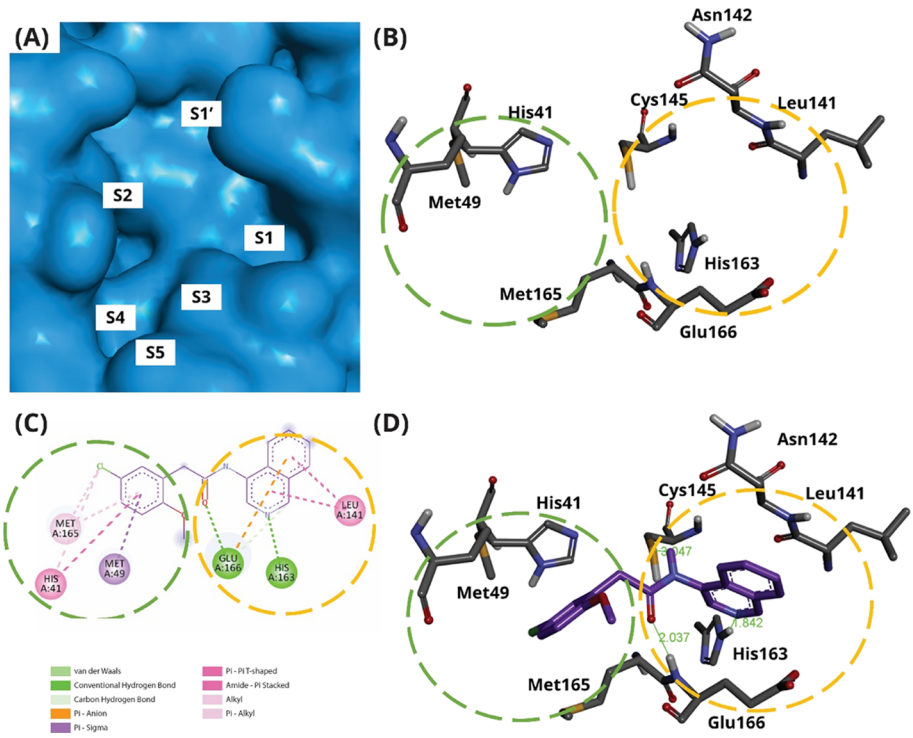

Figure 1. Illustration of the SARS-CoV-2 Mpro binding site and the main interaction subsites using Discovery Studio Visualizer (PDB ID: 7S3K): (A) 3D model of Mpro binding pocket with the subpockets location being labeled such as S1, S2, S3, S4, S5, and subunit S1′. (B) Key residues in S1 (yellow dashed line) and S2 (green dashed line). (C) 2D illustration of the interactions between Mpro and a noncovalent inhibitor (Z1530718726, purple, IC_{50} = 1.8 μM) (PDB ID: 7S3K) with the S1 and S2 being circled in yellow and green, subsequently. (D) Z1530718726 (purple) in the binding site with the key residues and its hydrogen bonds shown as green lines. The subsites S1 and S2 are circled in yellow and green, respectively.

phytochemicals with the Mpro inhibiting activity (such as myricetin with the IC_{50} value being 3.68 μM, dihydromyricetin with IC_{50} being 1.14 μM, quercetagetin with IC_{50} being 1.24 μM, and baicalein with IC_{50} being 0.94 μM).[12] With many advantages of natural substances in drug discovery and development,[13,14] the identification of natural SARS-CoV-2 Mpro inhibitors may lead to the development of effective therapeutic agents against the COVID-19 pandemic. Moreover, as a hot target for revealing novel anti-SARS-CoV-2 agents, a plethora of inhibitors targeting Mpro was discovered in a wide range of research (such as the COVID Moonshot initiative, HTS studies, and drug repurposing studies).[7,12,15−17] As a result, more than 600 3D co-crystal structures of Mpro with the inhibitors (both covalent and noncovalent) were revealed. However, utilizing the information offered by those structures to search for new inhibitors remains finite.

With that in mind, we aimed to explore novel natural noncovalent inhibitors through structure-based approaches. Initially, by closely inspecting 223 co-crystal complexes gathered from studies and the COVID Moonshot initiative (Supplement data 1),[15] the properties of the Mpro binding site were analyzed to generate a structure-based 3D-pharmacophore model. The model was then applied to identify novel natural noncovalent inhibitors from our in-house natural substance database (Supplement data 2). In order to understand the binding interactions between the hits and Mpro, induced-fit molecular docking with the employment of the pharmacophore model was performed by the Dock module in MOE (version 2022.02). Due to the limitation of the scoring function in molecular docking,[18] by combining the OnionNet2 interaction fingerprints generated with the deep learning module in RapidMiner (Educational version 9.10.007),[19] a machine-learning-based activity prediction model was employed to determine the best substances.

2. RESULTS AND DISCUSSION

2.1. 3D-Pharmacophore Development. *2.1.1. 3D-Pharmacophore Generation.* Although a plethora of co-crystal structures of Mpro in complex with inhibitors have been revealed recently, utilizing them to develop structure-based pharmacophore models remains finite. So far, most structure-based pharmacophore models for Mpro inhibitors have only been generated based on a handful of complexes,[20−24] which might not fully represent typical Mpro inhibitors. Moreover, in some cases, pharmacophore models with only noncovalent features have been built by mixtures of different groups of inhibitors, despite the differences in their inhibition mechanisms. Hence, in this study, we used a large number of Mpro structures in complexes with noncovalent inhibitors (223 complexes) to identify the characteristics of typical Mpro noncovalent inhibitors and applied them to screen for potential natural inhibitors from our library of compounds isolated from Vietnamese herbals.

Initially, 223 co-crystal structures of SARS-CoV-2 Mpro with inhibitors were closely inspected individually using Discovery Studio Visualizer to explore the interaction properties (hydrogen bond, ionic bond, and hydrophobic interaction) of the Mpro binding site when it interacts with noncovalent inhibitors. By mapping out the patterns of interactions in the binding site (Supplement data 1), it is clear that S1 and S2 are the two key interaction sites of the Mpro binding site (Figure 1A).

https://doi.org/10.1021/acsomega.2c07259
ACS Omega 2023, 8, 6679−6688

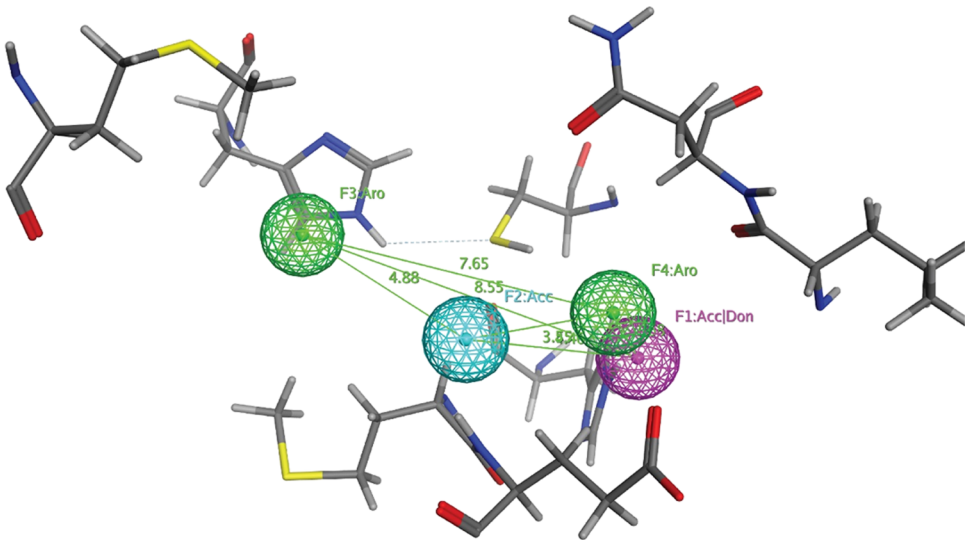

Figure 2. Pharmacophore model (model A) of Mpro noncovalent inhibitors represents the required interactions for inhibiting Mpro in the binding site.

From our analysis, S1 can be characterized as a shallow hydrophilic pocket with the key residues being Leu141, Asn142, Cys145 (the catalyst dyad), His163, and Glu166 (Figure 1B). No ionic bond between Mpro and inhibitor was recorded in 223 complexes. Additionally, as binding with His163 through a hydrogen bond is crucial, baicalein is the only case that can indirectly form a hydrogen bond with His163 through a water molecule.[25] However, as the direct bond with His163 occurs in all other cases, it is the go-to characteristic of potential Mpro inhibitors. From our observation, there was also a nonclassical hydrogen bond formation between Cys145 and noncovalent inhibitors, in which the thiol group of Cys145 acted as a hydrogen bond acceptor (Figure 1D). Despite this, the bond was considered more coincident than crucial since the bond lengths in most cases were too high (3.30−4.00 Å) compared to a typical hydrogen bond (2.70−3.30 Å).[26] Curiously, most of the noncovalent inhibitors (217 compounds) were also favored in forming a hydrophobic interaction (π-amid) with the amid bridge connecting Leu141 with Asn142 by using an arene subunit, which is in agreement with the structure−activity relationship result released by the Moonshot initiative—an increase in potency due to picking up additional hydrophobic interaction with Asn142.[15]

On the other hand, the S2 pocket seems to have a much more hydrophobic nature, with the dominant interactions being $\pi-\pi$ stacking formed by the sidechain of His41 (the catalyst dyad) and alkyl interactions with the sidechain of Met49 and Met165 with the arene subunit of inhibitors (Figure 1C,D).

In conclusion, a typical Mpro noncovalent inhibitor should have four main features, (i) having a hydrophobic arene subunit in the S2 site; (ii) and (iii) forming hydrogen bonds with the sidechain of His163 (usually through an acceptor) and Glu166 (through an acceptor); and (iv) having an arene group in the S1 pocket. These results concurred with many previous reports on the structural basis of potential inhibitors targeting SARS-CoV-2 Mpro and the experimental data released by the COVID Moonshot initiative.[15,27] From the four key features, the 3D-pharmacophore model (A) representing the typical Mpro noncovalent inhibitors was generated using the Pharmacophore Query Editor of MOE (Figure 2). As a result, the pharmacophore hypothesis supported by experimental data provided the information to discover and design new Mpro inhibitors.

The purple query is hydrogen acceptor or hydrogen donor (Acc/Don) (forming a hydrogen bond with His163 sidechain), the green query is arene subunit (Aro) ($\pi-\pi$ stacking interaction with His41 and an arene subunit in S1), and the cyan one is hydrogen acceptor (Acc) (forming a hydrogen bond with Glu166 backbone).

2.1.2. 3D-Pharmacophore Validation and Refinement. In order to assess the ability to identify and distinguish active compounds from inactive ones, the pharmacophore model A was validated by screening a test set. The model validation result is illustrated in Table 1.

Despite the high sensitivity in identifying active compounds (Se = 94.74%), the model is inadequate for the inactive one (Sp = 80.54%). As a result, the accuracy and the GH score of

Table 1. Validation Result of Pharmacophore Models (A and B)

	model A	model B
number of active compounds (A)	190	
number of inactive compounds (I)	1264	
hits (Ht)	426	296
active hits (Ha)	180	175
sensitivity (Se)	94.74%	92.11%
specificity (Sp)	80.54%	**90.42%**[b]
accuracy (Acc)	82.39%	**90.65%**
goodness-of-hit (GH) score[a]	0.45	**0.61**

[a]$\mathrm{GH} = \left(\frac{Ha \times (3A + Ht)}{4 \times Ht \times A}\right) \times \left(1 - \frac{Ht - Ha}{I}\right)$.[28] Generally, if the GH score is between 0.16 (score of a typical bad model) and 0.50 (score of a typical good model), the model is considered an average one.[28] In the case of a good pharmacophore model, its GH score should be 0.50 or higher.[28] [b]The boldface values illustrate the improvement of the pharmacophore model after refinement (comparing the refined model B with the original model A). There is an increase of 9.88% (roughly 10%) in the specificity, 8.26% in the total accuracy, and from 0.45 to 0.61 in the GH score.

https://doi.org/10.1021/acsomega.2c07259
ACS Omega 2023, 8, 6679−6688

model A are 82.39% and 0.45, which indicate the insufficient screening ability to search for potential Mpro inhibitors as an average model. In order to have a more competent pharmacophore model, model refinement was conducted. In order to keep the high sensitivity while increasing the ability to remove inactive substances from the screening result, the exclusion volume was employed to put the shape of the binding site into consideration by using the volume feature in the Query Editor of MOE. Since the binding site of Mpro is a flexible site,[15] each region exclusion volume tolerance was manually fine-tuned based on the information from the COVID Moonshot initiative,[15] which in turn led to the development of the refined pharmacophore model (B) (Figure 3).

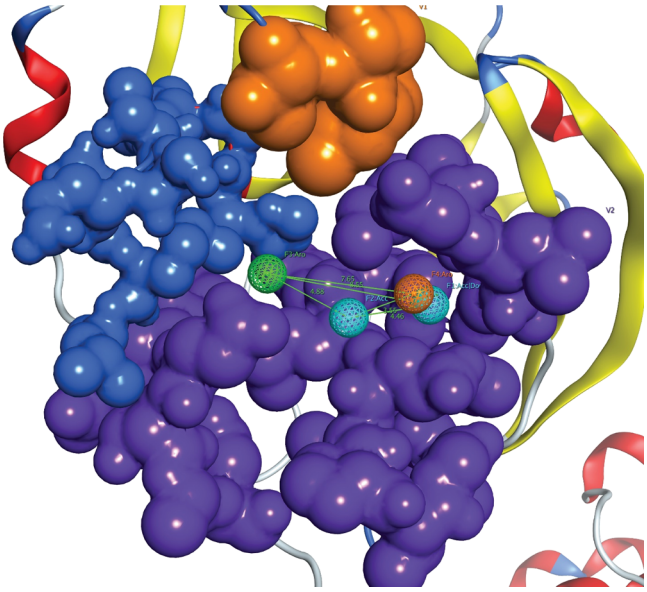

Figure 3. Refined pharmacophore model (model B).

Model B consists of four main features of typical Mpro noncovalent inhibitors (i) having a hydrophobic arene subunit in the S2 site; (ii) and (iii) forming hydrogen bonds with the sidechain of His163 and Glu166; and (iv) having an arene group in the S1 pocket and exclusion volumes. The orange exclusion volumes represent the S1′ site (the tolerance being 1.80 Å), the purple exclusion volumes represent the S1, S3, S4, and S5 sites (the tolerance being 1.50 Å), while the remaining (S2) was represented by blue exclusion volumes (the tolerance being 1.10 Å).

Model B was validated by the same process as model A. The validation result and the comparison between model A and model B are illustrated in Table 1. As the main primary objective of the pharmacophore model in this study is to search for potentially suitable candidates to inhibit Mpro, prioritizing specificity over sensitivity is reasonable. Hence, the benefit of removing more inactive substances (Sp increased to 90.42%) outweighed the slight drop in sensitivity (Se decreased to 92.11%). Moreover, due to the rise in the model GH score (from 0.45 to 0.61), the refined model (model B) is considered a good model. Therefore, model B was selected to screen for potential Mpro noncovalent inhibitors.

2.1.3. Pharmacophore-Based Virtual Screening. Using the Pharmacophore Search module in MOE, a pharmacophore-based virtual screening process was performed to identify potential Mpro noncovalent inhibitors in our in-house database, consisting of 273 phytochemicals extracted from Vietnamese herbals. As a result, we obtained 18 substances, 5 of which had been assayed *in vitro* (Table 2). Interestingly,

Table 2. Phytochemicals and/or Their Derivatives That Were In Vitro Assayed

compound	IC_{50} (μM)	derivative	IC_{50} (μM)	reference
catechin		(+)-catechin-3-*O*-gallate	2.98	29
(+)-catechin	inactive			
epicatechin	inactive	(−)-epicatechin-3-*O*-gallate	5.21	29
ampelopsin	1.716			30
quercetin	192	8-(*p*-tolylselenyl) quercetin	8	31

most of the compounds retrieved were flavonoids and lignans, which were in agreement with the report of many SARS-CoV-2 Mpro natural inhibitors being flavonoids, such as myricetin (IC_{50} = 0.63 μM), dihydromyricetin (IC_{50} = 1.14 μM), baicalein (IC_{50} = 0.94 μM), etc.[12]

2.2. Molecular Docking and Activity Prediction. *2.2.1. Induced-Fit Molecular Docking.* Since 5 of 18 hits were explored *in vitro*, the remaining 13 compounds were examined by molecular docking to investigate the ability to bind to Mpro. The extracted protein structures of Mpro in monomeric (PDB ID: 7L11) and dimeric forms (PDB ID: 7D3I) were downloaded from the protein databank. Due to the flexibility of the binding site,[15] induced-fit molecular docking was selected to put that into consideration, using the Dock module in MOE (version 2022.02). As the pharmacophore model development highlights four key residues interacting with Mpro noncovalent inhibitors, His41, Leu141, His163, and Glu166, interacting with them are the main criteria in the analysis of the docking results. As Mpro exists in dimeric and monomeric forms, we also compared their differences regarding how the hits interacted with them. Despite having all the required features, the docking results in monomeric and dimeric Mpro showed that isoxanthohumol could not follow the pharmacophore orientation when bound to the Mpro binding site, while the other 12 neatly could. Besides interactions, the binding affinities, mostly under −6.00 kcal/mol, indicated that most hits could fit quite well with the binding site.

There were no significant differences between the conformations of most hits when they bound with monomeric and dimeric Mpro (RMSD < 2.0 Å) (Table 3). On top of this, most of them also had similar binding affinities (Table 3) and interactions (Tables S1 and S2) when bound to Mpro in both forms with the *p*-value > 0.5. Hence, the changes in the Mpro structure due to the dimerization occurring in domains II and III (residues 201−306) of each Mpro monomer unit only had minor effects on how the catalytic site, located in chymotrypsin-like domains I (residues 8−101) and II (residues 102−184), interacted with the hits. Noticeably all other 12 natural substances can form proper interactions with the four key residues (Tables S1 and S2). Regarding the one unique case, calycosin-7-*O*-β-glucopyranoside, which had two different conformations when bound with monomeric and dimeric Mpro, the differences came from how its β-glucopyranose subunit interacted with the binding site. When

https://doi.org/10.1021/acsomega.2c07259
ACS Omega 2023, 8, 6679−6688

Table 3. Comparison of the Hits' Conformations When They Bind to Monomeric and Dimeric Mpro

compound	binding affinity with monomeric Mpro (kcal/mol)	binding affinity with dimeric Mpro (kcal/mol)	RMSD (Å)
12*a*-hydroxyelliptone	−6.36	−6.37	0.8784
calycosin	−5.91	−5.73	0.2563
calycosin-7-*O*-*β*-glucopyranoside	−8.33	−6.93	4.9780
dihydrorhamnocitrin	−5.35	−5.39	0.6175
eudesmin	−7.91	−8.05	0.5807
huazhongilexin	−7.81	−7.29	0.5030
loureirin	−6.18	−5.88	0.7557
niranthin	−8.29	−8.63	0.8482
p-coumaroyltyramin	−6.23	−5.55	0.9534
phyllanthin	−8.06	−8.40	0.6975
nigracin	−6.95	−6.67	1.3828
syringaresinol	−7.85	−7.15	0.4135

bound to dimeric Mpro, calycosin-7-*O*-*β*-glucopyranoside inserted its *β*-glucopyranose subunit deep into the S2 subpocket instead of expanding its interactions to the S4 subsite (Figure S1). However, due to the S2 hydrophobic nature, the interactions between calycosin-7-*O*-*β*-glucopyranoside and dimeric Mpro required further study to be confirmed.

2.2.2. Machine-Learning Activity Prediction Modeling. In order to overcome the limitation of the docking scoring function and rank the hits efficiently, activity prediction models based on interaction fingerprints were developed using 223 co-crystal complexes of Mpro with noncovalent inhibitors by OnionNet2 and RapidMiner (Educational version 9.10.007).[19] The 3D structures were converted into interaction fingerprints by OnionNet2. Applying the Stratified sampling method in RapidMiner, the data set was split into the training set and test set in two different ratios, 70:30 and 80:20. Table 4 illustrates

Table 4. Validation of Activity Prediction Models for Noncovalent SARS-CoV-2 Mpro Inhibitors on the Test Set

model	training set:test set ratio	RMSE[a]	*R*	R^2
ML1	70:30	0.662	0.64	0.41
ML2	80:20	0.532	0.81	0.65

[a]RMSE: root-mean-square deviation.

the effect of changing the ratio between the training set and the test set on the model performances. With the finite data, the larger the training set size, the better the model performance. From the results, model ML2 was selected to rank potential Mpro noncovalent natural inhibitors.

From the activity prediction results using ML2 (Table 5), calycosin-7-*O*-*β*-glucopyranoside and nigracin were the ones that have the predicted IC_{50} being nanomolar concentration level. This result was reasonable as both potent hits have many similarities with highly potent Mpro inhibitors (ensiltrelvir) in terms of interacting with Mpro (Figure S2). Intriguingly, in the case of calycosin-7-*O*-*β*-glucopyranoside (glycoside form), compared to calycosin (aglycon form), calycosin-7-*O*-*β*-glucopyranoside was more competent in both the ability to bind to the binding site (having the best binding affinity) and the ability to inhibit Mpro predicted by ML2 (predicted IC_{50} = 0.549 *μ*M). This improvement could be explained by expanding calycosin-7-*O*-*β*-glucopyranoside interaction sites

Table 5. Activity Prediction Result for the Examined Hits

compounds	predicted IC_{50} (*μ*M)
nigracin	0.475
calycosin-7-*O*-*β*-glucopyranoside	0.549
12*a*-hydroxyelliptone	1.313
calycosin	1.919
loureirin	2.455
p-coumaroyltyramin	2.524
syringaresinol	2.673
dihydrorhamnocitrin	3.096
huazhongilexin	3.102
niranthin	3.219
eudesmin	4.420
phyllanthin	17.508

on Mpro to the subpocket S4 using the glucose subunit (Figure 4).

2.3. Toxicity, Physicochemical Property, Drug-Likeness, and Pharmacokinetic Predictions. About calycosin-7-*O*-*β*-glucopyranoside, there were some *in vitro* and *in vivo* studies on its toxicity and pharmacokinetics. Regarding toxicity, calycosin-7-*O*-*β*-glucopyranoside is also considered low toxicity, with the CC_0 and CC_{50} values to Vero cells being 125 and 143 mg/mL.[32] In terms of oral and intestinal absorptions, the calculated bioavailability of oral calycosin-7-*O*-*β*-glucoside was only 0.304% due to the presence of glucoside hydrolase in the intestine.[33] However, the drug time curve of intraperitoneally injected calycosin-7-*O*-*β*-glucoside and its metabolites was entirely different from that of oral calycosin-7-*O*-*β*-glucoside.[33] Moreover, the metabolism product of calycosin-7-*O*-*β*-glucoside with the presence of glucoside hydrolase is calycosin, which was also predicted as a noncovalent Mpro inhibitor in this study (predicted IC_{50} = 1.919 *μ*M). Hence, calycosin-7-*O*-*β*-glucopyranoside is still considered a drugable substance in terms of injection.

As there were only a handful of studies on the toxicity, physicochemical properties, drug-likeness, and pharmacokinetics of nigracin, ProTox-II and SwissADME web servers were used to predict that information (Table 6).[34,35] First and foremost, nigracin does not violate Lipinski's rule of five (MW ≤ 500, NHBAs ≤ 10, NHBDs ≤ 5, Log $P_{o/w}$ ≤ 4.15), indicating its drug-likeness nature. Despite not violating Lipinski's rule of five, due to the high TPSA and water solubility, the predicted gastro-intestine absorption of both hits was considered low. This result can be explained by the presence of a sugar subunit in nigracin's structure, which is common in many natural substances. Although oral administration seemed unfeasible for nigracin, other forms of administration were still possible for nigracin. In terms of toxicity, from the results (Table 6), nigracin was predicted as a low-toxicity substance, with a high predicted LD_{50} (2190 mg/kg) and not acting as any form of hepatotoxicity, carcinogenicity, or immunotoxicity. On top of this, the metabolism prediction also showed that nigracin did not act as a drug transporter of P-glycoprotein substrate nor interact with a wide range of hepatic enzymes. Thus, nigracin was considered a low-safety risk compound with a neglectable chance of causing drug−drug interactions.

Overall, starting with 223 complexes of Mpro with noncovalent inhibitors, we have successfully employed a combination of *in silico* methods, including pharmacophore modeling, induced-fit molecular docking, and machine learning

https://doi.org/10.1021/acsomega.2c07259
ACS Omega 2023, 8, 6679−6688

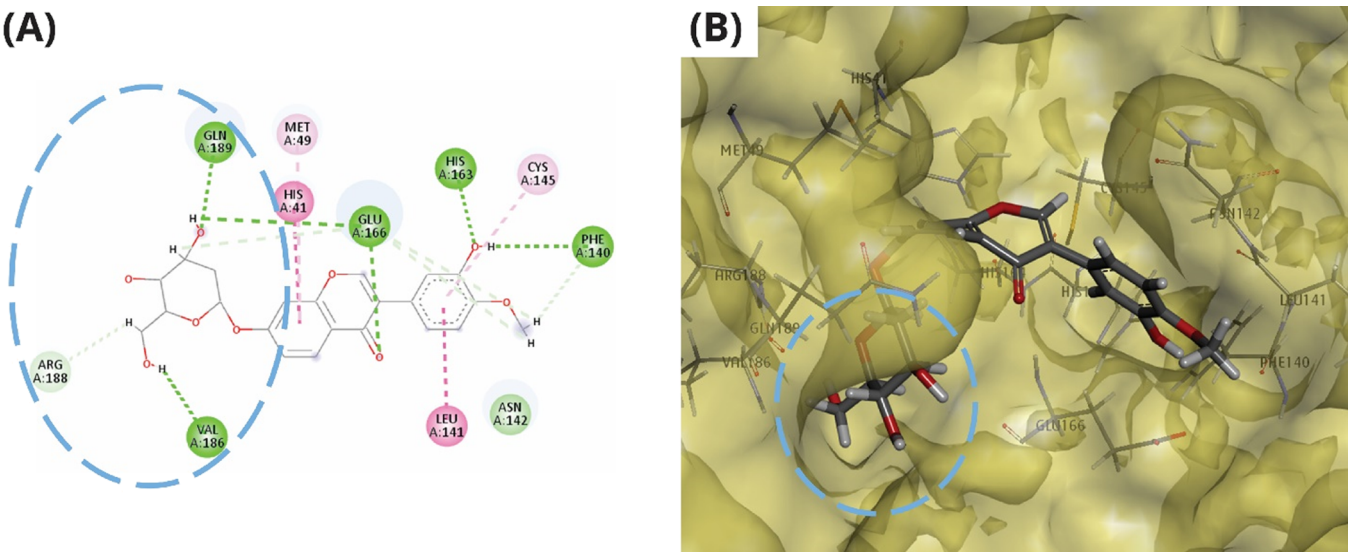

Figure 4. (A) 2D illustration of interactions between calycosin-7-*O*-*β*-glucopyranoside and Mpro with the expansion interaction subsite (S4) circled in blue. (B) Calycosin-7-*O*-*β*-glucopyranoside in the binding site of Mpro with the expansion interaction subsite (S4) circled in blue.

Table 6. Toxicity, Physicochemical Property, and Pharmacokinetic Prediction Results

properties	value	properties	value
molecular weight (MW)	406.38 g/mol	CYP1A2 inhibitor	no
NHBAs[a]	9	CYP2C19 inhibitor	no
NHBDs[a]	5	CYP2C9 inhibitor	no
consensus Log $P_{o/w}$	0.33	CYP2D6 inhibitor	no
solubility[b]	soluble	CYP3A4 inhibitor	no
TPSA[a]	145.91 Å^2	hepatotoxicity	inactive
GI absorption[a]	low	carcinogenicity	inactive
blood−brain barrier permeant	no	immunotoxicity	inactive
predicted LD_{50}	2190 mg/kg	mutagenicity	inactive
toxicity class[c]	V	cytotoxicity	inactive
P-glycoprotein substrate	no		

[a]NHBAs: number of hydrogen bond acceptors; NHBDs: number of hydrogen bond donors; TPSA: topological polar surface area; and GI absorption: gastro-intestine absorption. [b]Based on predicted Log *S*, the solubility of a substance is classified into six classes: insoluble < −10 < poorly soluble < −6 < moderately soluble < −4 < soluble < −2 < very soluble <0 < highly soluble.[34] [c]From the toxicity doses (LD_{50}), there are six toxicity classes indicating how poisonous a compound can be.[35] The indications are fatal if swallowed (I and II), toxic if swallowed (III), harmful if swallowed (IV), may be harmful if swallowed (V), and nontoxic (VI).[35]

to screen for potential hits. The novelty of our study mostly came from our library of compounds isolated from Vietnamese herbals.

3. CONCLUSIONS

In this work, we employed a combination of structure-based strategies to utilize the vastly available co-crystal structures of Mpro with noncovalent inhibitors published recently to get insight into the Mpro inhibition and explore the potential leads. By closely inspecting 223 structures of Mpro with noncovalent inhibitors, four key residues were revealed, His41, Leu141, His163, and Glu166, which in turn led to the generation of the four-feature structure-based 3D-pharmacophore model (two arenes, one hydrogen bond acceptor, and one hydrogen bond donor or acceptor). Afterward, the model was validated by experimental data and refined to have decent validation scores (sensitivity = 92.11%, specificity = 90.42%, accuracy = 90.65%, and goodness-of-hit score = 0.61) before being applied in the *in silico* screening. The hits were then investigated by induced-fit molecular docking before being ranked by a machine-learning interaction-fingerprints-based activity predicting model. As a result, two potent natural inhibitors were suggested, calycosin-7-*O*-*β*-glucopyranoside (predicted IC_{50} = 0.549 *μ*M) and nigracin (predicted IC_{50} = 0.475 *μ*M). However, as this was an *in silico* study, further experimental assays would be required to confirm the anti-Mpro activities of the obtained hits. In conclusion, besides the virtual screening hits, this research provided additional insight into the inhibition of Mpro by noncovalent inhibitors, complementing the work of experimental research and opening the opportunity for developing new SARS-CoV-2 antivirals.

4. MATERIALS AND METHODS

4.1. Material. In this study, 223 co-crystal structures of Mpro with noncovalent inhibitors from the COVID Moonshot initiate and publications (PDB ID: 5RGX, 5RH3, 5RHD, 6M2N, 6W63, 7KX5, 7L0D, 7L10, 7L11, 7L12, 7L13, 7L14, 7LMD, 7LME, 7LMF, 7LTJ, 7P2G, 7P51, 7S3K, 7S3S, 7S4B, 7VTH, and 7VU6) were downloaded and analyzed (Supplement data 1). A database of 8702 substances with Mpro percentage inhibition at 20 *μ*M (ChEMBL ID: CHEMBL4495564) was utilized.[17] The database used for screening was the in-house database that contains 273 Vietnamese natural compounds (Supplement data 2).

4.2. Methods. Overall, the study followed the workflow described in Figure 5, from the pharmacophore modeling to the hit ranking by a machine-learning activity prediction model.

4.2.1. 3D-Pharmacophore Development and Application. Initially, 223 complexes of Mpro with inhibitors were examined individually using Discovery Studio Visualizer

https://doi.org/10.1021/acsomega.2c07259
ACS Omega 2023, 8, 6679−6688

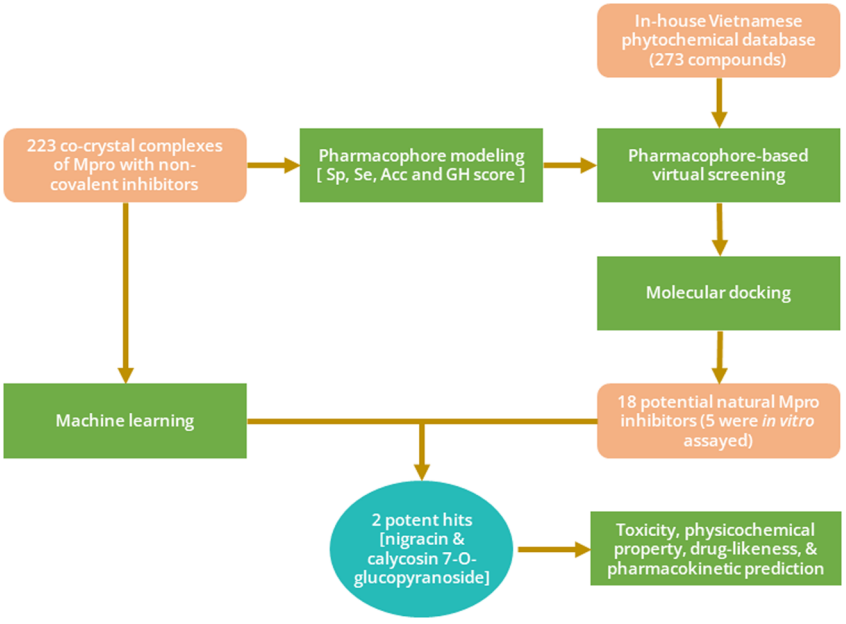

Figure 5. Overall workflow for the screening procedure.

2021. The key ligand−receptor interactions were identified and confirmed from the analyzed result, which led to the generation of the 3D-pharmacophore model using the Query Editor module in MOE (version 2022.02).

In order to test the ability to distinguish active compounds from others, the generated pharmacophore model was validated by screening a test set using the Pharmacophore Search module in MOE (version 2022.02). The test set consists of 190 Mpro noncovalent potent inhibitors, with the IC_{50} being 20 μM or lower and 1264 confirmed noninhibitors. The active compounds in the test set were extracted from the co-crystal complexes. The inactive ones were extracted from 8702 compounds with Mpro percentage inhibition at 20 μM (inhibiting Mpro 2% or lower at 20 μM).[17] The compounds in the test set were conformation generated in MOE (Conformation Import) before being applied in the validation step. In the Conformation Import tool, Conformations was set to 10,000, Refinement Conformation Limit was 300, Stochastic Search Failure Limit was 1000, Stochastic Search Iteration Limit was 1000, Energy Minimization Iteration Limit was 1000, and Energy Minimization Gradient Test was 0.0001.

Regarding the pharmacophore model's predicting accuracy, the model's quality was validated by a test set consisting of *in vitro*-confirmed active (190 substances) and inactive compounds (1264 substances). The criteria used were sensitivity (Se), specificity (Sp), accuracy (Acc), and goodness-of-hit score (GH score). Se (percentage of true positives in the positive hits), Sp (percentage of true negatives in the negative hits), and Acc (percentage of accurate predictions in the total prediction) scored the correct prediction percentage when applying the model to a test set. In order to minimize the effect of the database size on the scoring results, the GH score and its interpretations were also used.[28] The GH score can be calculated by using this formula:[28]

$$GH = \left(\frac{Ha \times (3 \times A + Ht)}{4 \times Ht \times A}\right) \times \left(1 - \frac{Ht - Ha}{I}\right)$$

Generally, if the GH score is between 0.16 (score of a typical bad model) and 0.50 (score of a typical good model), the model is considered average.[28] In the case of a good pharmacophore model, its GH score should be 0.50 or higher.[28]

In order to refine the pharmacophore model, the exclusion volumes representing the binding site were added using the volume feature in the Query Editor module and revalidated the refined model. Once the refined pharmacophore model satisfied the criteria of being good (GH score > 0.5), it would be considered the final model.

Afterward, the obtained final model was used as a blueprint to explore potential Mpro natural noncovalent inhibitors using the Pharmacophore Search module in MOE (version 2022.02). The database used in the virtual screening was the in-house database, which contains 273 Vietnamese natural substances (Supplement data 2).

4.2.2. Induced-Fit Molecular Docking. Due to the flexibility of the binding site of Mpro,[15] induced-fit molecular docking was selected to put that into consideration, using the Dock module in MOE (version 2022.02). The extracted protein structures of Mpro in monomeric (PDB ID: 7L11) and dimeric forms (PDB ID: 7D3I) were downloaded from the protein databank. Using the MOE program (version 2022.02), the protein structures of Mpro were then prepared by removing water, ligand, and ions before protonating the system. In the protonate 3D module, the setting was set at the pH being 7.4 and the default setting for the others. Using the Site Finder tool and the experimental data of the binding site location from co-crystal complexes, the binding site of Mpro, which contains the catalyst dyads, was defined as dummy atoms in MOE. The ligands were protonated and energy minimized by the energy minimized module in MOE, with the setting of gradient being 0.0001, while the other settings were default.

In the docking setting, the receptor was set as MOE, all atoms; site as dummy atoms; pharmacophore as PH4 file; ligand as MDB file; placement as pharmacophore with the timeout (second) being 3600 and no. of return poses being 20,000; refinement as induced fit with the sidechain being free; The score as default (London dG and GBVI/WSA dG) with

https://doi.org/10.1021/acsomega.2c07259
ACS Omega 2023, 8, 6679−6688

the output poses being 100 (for London dG) and 10 (for GBVI/WSA dG). The results were validated individually based on how they interacted with Mpro using the information described by the pharmacophore model. Docking results were validated based on the binding interactions forming by Mpro and ligands. These binding interactions were analyzed regarding the chemical features taken from the generated pharmacophore above. The differences between the ligands when they interacted with monomeric and dimeric Mpro were also validated by the RMSD values. The RMSD values between the hits when they bound to two forms of Mpro were calculated by using Biovia Discovery Studio Visualizer.

4.2.3. Machine-Learning Interaction-Fingerprint-Based Activity Predicting Modeling. Although molecular docking has a crucial role in structure-based drug discovery and design, there are still some flaws,[36] one of which is the false positives from ranking ligands due to the prioritization of the rapid screening speed over accurate binding affinity prediction of the method.[18,36] Thus, activity prediction models based on interaction fingerprints were developed to rank the hits efficiently by OnionNet2 and RapidMiner (Educational version 9.10.007) using 223 co-crystal complexes of Mpro with noncovalent inhibitors.[19]

Initially, 223 complexes of Mpro with inhibitors were protonated by MOE (version 2022.02) with the pH = 7.4 and the default setting for the others. Afterward, the interaction fingerprints of 223 complexes (input database) were generated by the OnionNet2 software.[19] The input database was split into two sets (training and test) by the split data module with two different ratios (70 training: 30 test and 80 training: 20 test), with the sampling method being stratified sampling (building random subsets and ensuring that the class distribution in the subsets is the same as in the whole input set). The training sets were then used to generate the machine-learning model, while their test counterparts were used to validate the models' accuracy. The models' forecasting abilities were scored based on three criteria RMSE (error between predicted results and experimental data), R, and R^2 (correlation between predicted results and experimental data). The model was considered predictable for virtual screening when its $R^2 > 0.5$.

The activity prediction models were developed by the deep learning expansion of RapidMiner (Educational version 9.10.007). The deep learning module was comprised of two hidden layers (32 neurons for the first layer and 16 neurons for the second one) being fully connected layers. The activator of each layer was set as ReLU (rectified linear unit). The machine learning process was set to 1000 epoch, 0.01 learning rate, while the other settings were set as default. After the model was generated, it was stored and applied to predict the test set for validation using Apply Model. Using the test set predicting results and the performance module in RapidMiner. The best model (with the lowest RMSE and highest R and R^2) was deployed using Apply Model to predict the hits.

4.2.4. Toxicity, Physicochemical Property, Drug-Likeness, and Pharmacokinetic Predictions. Besides the ability to inhibit the target, toxicity and drug-like properties have also been critical factors in the success of drug development.[37] As unmanageable toxicity and poor drug-like properties contribute to 30 and 10−15% of clinical failures of drug development,[37] it is necessary to study the toxicity, physicochemical property, drug-likeness, and pharmacokinetics of potent substances. In order to study the toxicity of the hits (including LD_{50}, toxicity class, hepatotoxicity, carcinogenicity, immunotoxicity, mutagenicity, and cytotoxicity), the ProTox-II web server was used.[35] In terms of physicochemical properties (number of hydrogen bond acceptors, number of hydrogen bond donors, Log $P_{o/w}$, water solubility, and topological polar surface area), drug-likeness (Lipinski's rule of five), and pharmacokinetics of the hits (gastro-intestine absorption, blood−brain barrier permeant, and hepatic enzyme inhibitions), they were predicted by the SwissADME web server.[34]

■ ASSOCIATED CONTENT

Supporting Information

The Supporting Information is available free of charge at https://pubs.acs.org/doi/10.1021/acsomega.2c07259.

Two tables describe the interaction between the hits and Mpro; a figure illustrates the differences between the conformations of calycosin-7-*O*-*β*-glucopyranoside binding to two forms of Mpro; and a figure illustrates the similarity between the potent hits (calycosin-7-*O*-*β*-glucopyranoside and nigracin) and a highly potent inhibitor (Ensitrelvir) (PDF)

Interactions between Mpro and 223 noncovalent inhibitors (XLSX)

In-house phytochemical database (XLSX)

■ AUTHOR INFORMATION

Corresponding Author

Phuong Thuy Viet Nguyen − *Faculty of Pharmacy, University of Medicine and Pharmacy at Ho Chi Minh City, Ho Chi Minh City 700000, Vietnam;* orcid.org/0000-0002-0233-8692; Phone: +084-919520708; Email: ntvphuong@ump.edu.vn

Author

Cuong Quoc Duong − *Faculty of Pharmacy, University of Medicine and Pharmacy at Ho Chi Minh City, Ho Chi Minh City 700000, Vietnam*

Complete contact information is available at: https://pubs.acs.org/10.1021/acsomega.2c07259

Notes

The authors declare no competing financial interest.

■ ACKNOWLEDGMENTS

This research did not receive any specific grant from funding agencies in the public, commercial, or not-for-profit sectors.

■ REFERENCES

(1) Cucinotta, D.; Vanelli, M. WHO Declares COVID-19 a Pandemic. *Acta Biomed.* **2020**, *91*, 157−160.

(2) WHO. WHO Coronavirus (COVID-19) Dashboard. https://covid19.who.int/ (accessed September 2022).

(3) CDC. COVID-19 Treatments and Medications. https://www.cdc.gov/coronavirus/2019-ncov/your-health/treatments-for-severe-illness.html (accessed September 2022).

(4) CDC. Interim Clinical Considerations for COVID-19 Treatment in Outpatients. https://www.cdc.gov/coronavirus/2019-ncov/hcp/clinical-care/outpatient-treatment-overview.html (accessed September 2022).

(5) WHO. Tracking SARS-CoV-2 variants. https://www.who.int/activities/tracking-SARS-CoV-2-variants (accessed September 2022).

(6) Wang, Q.; Guo, Y.; Iketani, S.; Nair, M. S.; Li, Z.; Mohri, H.; Wang, M.; Yu, J.; Bowen, A. D.; Chang, J. Y.; Shah, J. G.; Nguyen, N.;

Chen, Z.; Meyers, K.; Yin, M. T.; Sobieszczyk, M. E.; Sheng, Z.; Huang, Y.; Liu, L.; Ho, D. D. Antibody evasion by SARS-CoV-2 Omicron subvariants BA.2.12.1, BA.4 and BA.5. *Nature* **2022**, *608*, 603−608.
(7) Macip, G.; Garcia-Segura, P.; Mestres-Truyol, J.; Saldivar-Espinoza, B.; Pujadas, G.; Garcia-Vallvé, S. A Review of the Current Landscape of SARS-CoV-2 Main Protease Inhibitors: Have We Hit the Bullseye Yet? *Int. J. Mol. Sci.* **2022**, *23*, 259.
(8) Kitamura, N.; Sacco, M. D.; Ma, C.; Hu, Y.; Townsend, J. A.; Meng, X.; Zhang, F.; Zhang, X.; Ba, M.; Szeto, T.; Kukuljac, A.; Marty, M. T.; Schultz, D.; Cherry, S.; Xiang, Y.; Chen, Y.; Wang, J. Expedited Approach toward the Rational Design of Noncovalent SARS-CoV-2 Main Protease Inhibitors. *J. Med. Chem.* **2022**, *65*, 2848−2865.
(9) Singh, J.; Petter, R. C.; Baillie, T. A.; Whitty, A. The resurgence of covalent drugs. *Nat. Rev. Drug Discovery* **2011**, *10*, 307−317.
(10) Bauer, R. A. Covalent inhibitors in drug discovery: from accidental discoveries to avoided liabilities and designed therapies. *Drug Discovery Today* **2015**, *20*, 1061−1073.
(11) Yamane, D.; Onitsuka, S.; Re, S.; Isogai, H.; Hamada, R.; Hiramoto, T.; Kawanishi, E.; Mizuguchi, K.; Shindo, N.; Ojida, A. Selective covalent targeting of SARS-CoV-2 main protease by enantiopure chlorofluoroacetamide. *Chem. Sci.* **2022**, *13*, 3027−3034.
(12) Antonopoulou, I.; Sapountzaki, E.; Rova, U.; Christakopoulos, P. Inhibition of the main protease of SARS-CoV-2 (Mpro) by repurposing/designing drug-like substances and utilizing nature's toolbox of bioactive compounds. *Comput. Struct. Biotechnol. J.* **2022**, *20*, 1306−1344.
(13) Atanasov, A. G.; Zotchev, S. B.; Dirsch, V. M.; Orhan, I. E.; Banach, M.; Rollinger, J. M.; Barreca, D.; Weckwerth, W.; Bauer, R.; Bayer, E. A.; Majeed, M.; Bishayee, A.; Bochkov, V.; Bonn, G. K.; Braidy, N.; Bucar, F.; Cifuentes, A.; D'Onofrio, G.; Bodkin, M.; Diederich, M.; Dinkova-Kostova, A. T.; Efferth, T.; El Bairi, K.; Arkells, N.; Fan, T.-P.; Fiebich, B. L.; Freissmuth, M.; Georgiev, M. I.; Gibbons, S.; Godfrey, K. M.; Gruber, C. W.; Heer, J.; Huber, L. A.; Ibanez, E.; Kijjoa, A.; Kiss, A. K.; Lu, A.; Macias, F. A.; Miller, M. J. S.; Mocan, A.; Müller, R.; Nicoletti, F.; Perry, G.; Pittalà, V.; Rastrelli, L.; Ristow, M.; Russo, G. L.; Silva, A. S.; Schuster, D.; Sheridan, H.; Skalicka-Woźniak, K.; Skaltsounis, L.; Sobarzo-Sánchez, E.; Bredt, D. S.; Stuppner, H.; Sureda, A.; Tzvetkov, N. T.; Vacca, R. A.; Aggarwal, B. B.; Battino, M.; Giampieri, F.; Wink, M.; Wolfender, J.-L.; Xiao, J.; Yeung, A. W. K.; Lizard, G.; Popp, M. A.; Heinrich, M.; Berindan-Neagoe, I.; Stadler, M.; Daglia, M.; Verpoorte, R.; Supuran, C. T.; The International Natural Product Sciences Taskforce. Natural products in drug discovery: advances and opportunities. *Nat. Rev. Drug Discovery* **2021**, *20*, 200−216.
(14) Bharadwaj, S.; Dubey, A.; Yadava, U.; Mishra, S. K.; Kang, S. G.; Dwivedi, V. D. Exploration of natural compounds with anti-SARS-CoV-2 activity via inhibition of SARS-CoV-2 Mpro. *Brief. Bioinform.* **2021**, *22*, 1361−1377.
(15) Consortium, T.; Chodera, J.; Lee, A.; London, N.; Delft, F.; Fernandes, R. *Open Science Discovery of Oral Non-Covalent SARS-CoV-2 Main Protease Inhibitors*; 2021.
(16) Jin, Z.; Du, X.; Xu, Y.; Deng, Y.; Liu, M.; Zhao, Y.; Zhang, B.; Li, X.; Zhang, L.; Peng, C.; Duan, Y.; Yu, J.; Wang, L.; Yang, K.; Liu, F.; Jiang, R.; Yang, X.; You, T.; Liu, X.; Yang, X.; Bai, F.; Liu, H.; Liu, X.; Guddat, L. W.; Xu, W.; Xiao, G.; Qin, C.; Shi, Z.; Jiang, H.; Rao, Z.; Yang, H. Structure of Mpro from SARS-CoV-2 and discovery of its inhibitors. *Nature* **2020**, *582*, 289−293.
(17) Kuzikov, M.; Costanzi, E.; Reinshagen, J.; Esposito, F.; Vangeel, L.; Wolf, M.; Ellinger, B.; Claussen, C.; Geisslinger, G.; Corona, A.; Iaconis, D.; Talarico, C.; Manelfi, C.; Cannalire, R.; Rossetti, G.; Gossen, J.; Albani, S.; Musiani, F.; Herzog, K.; Ye, Y.; Giabbai, B.; Demitri, N.; Jochmans, D.; Jonghe, S. D.; Rymenants, J.; Summa, V.; Tramontano, E.; Beccari, A. R.; Leyssen, P.; Storici, P.; Neyts, J.; Gribbon, P.; Zaliani, A. Identification of Inhibitors of SARS-CoV-2 3CL-Pro Enzymatic Activity Using a Small Molecule in Vitro Repurposing Screen. *ACS Pharmacol. Transl. Sci.* **2021**, *4*, 1096−1110.
(18) Wang, D. D.; Chan, M.-T.; Yan, H. Structure-based protein−ligand interaction fingerprints for binding affinity prediction. *Comput. Struct. Biotechnol. J.* **2021**, *19*, 6291−6300.
(19) Wang, Z.; Zheng, L.; Liu, Y.; Qu, Y.; Li, Y. Q.; Zhao, M.; Mu, Y.; Li, W. OnionNet-2: A Convolutional Neural Network Model for Predicting Protein-Ligand Binding Affinity Based on Residue-Atom Contacting Shells. *Front. Chem.* **2021**, *9*, No. 753002.
(20) Kumar, B. K.; Faheem; Sekhar, K. V. G. C.; Ojha, R.; Prajapati, V. K.; Pai, A.; Murugesan, S. Pharmacophore based virtual screening, molecular docking, molecular dynamics and MM-GBSA approach for identification of prospective SARS-CoV-2 inhibitor from natural product databases. *J. Biomol. Struct. Dyn.* **2022**, *40*, 1363−1386.
(21) Yin, S.; Mei, S.; Li, Z.; Xu, Z.; Wu, Y.; Chen, X.; Liu, D.; Niu, M.-M.; Li, J. Non-covalent cyclic peptides simultaneously targeting Mpro and NRP1 are highly effective against Omicron BA.2.75. *Front. Pharmacol.* **2022**, *13*, No. 1037993.
(22) Hassan, A.; Arafa, R. K. On the search for COVID-19 therapeutics: identification of potential SARS-CoV-2 main protease inhibitors by virtual screening, pharmacophore modeling and molecular dynamics. *J. Biomol. Struct. Dyn.* **2022**, *40*, 7815−7828.
(23) Vázquez-Mendoza, L. H.; Mendoza-Figueroa, H. L.; García-Vázquez, J. B.; Correa-Basurto, J.; García-Machorro, J. In Silico Drug Repositioning to Target the SARS-CoV-2 Main Protease as Covalent Inhibitors Employing a Combined Structure-Based Virtual Screening Strategy of Pharmacophore Models and Covalent Docking. *Int. J. Mol. Sci.* **2022**, *23*, 3987.
(24) Kanhed, A. M.; Patel, D. V.; Teli, D. M.; Patel, N. R.; Chhabria, M. T.; Yadav, M. R. Identification of potential Mpro inhibitors for the treatment of COVID-19 by using systematic virtual screening approach. *Mol. Diversity* **2021**, *25*, 383−401.
(25) Su, H.-X.; Yao, S.; Zhao, W.-F.; Li, M.-J.; Liu, J.; Shang, W.-J.; Xie, H.; Ke, C.-Q.; Hu, H.-C.; Gao, M.-N.; Yu, K.-Q.; Liu, H.; Shen, J.-S.; Tang, W.; Zhang, L.-K.; Xiao, G.-F.; Ni, L.; Wang, D.-W.; Zuo, J.-P.; Jiang, H.-L.; Bai, F.; Wu, Y.; Ye, Y.; Xu, Y.-C. Anti-SARS-CoV-2 activities *in vitro* of Shuanghuanglian preparations and bioactive ingredients. *Acta Pharmacol. Sin.* **2020**, *41*, 1167−1177.
(26) McRee, D. E. Computational Techniques. In *Practical Protein Crystallography*, 2nd edition; McRee, D. E., Ed.; Academic Press: San Diego, 1999; p 91.
(27) Mengist, H. M.; Dilnessa, T.; Jin, T. Structural Basis of Potential Inhibitors Targeting SARS-CoV-2 Main Protease. *Front. Chem.* **2021**, *9*, No. 622898.
(28) Güner, O. F. *Pharmacophore Perception, Development and Use in Drug Design*; International University Line, 2000; Vol 2, pp 195−210.
(29) Zhu, Y.; Xie, D. Y. Docking Characterization and *in vitro* Inhibitory Activity of Flavan-3-ols and Dimeric Proanthocyanidins Against the Main Protease Activity of SARS-Cov-2. *Front. Plant Sci.* **2020**, *11*, No. 601316.
(30) Xiao, T.; Wei, Y.; Cui, M.; Li, X.; Ruan, H.; Zhang, L.; Bao, J.; Ren, S.; Gao, D.; Wang, M.; Sun, R.; Li, M.; Lin, J.; Li, D.; Yang, C.; Zhou, H. Effect of dihydromyricetin on SARS-CoV-2 viral replication and pulmonary inflammation and fibrosis. *Phytomedicine* **2021**, *91*, 153704−153704.
(31) Mangiavacchi, F.; Botwina, P.; Menichetti, E.; Bagnoli, L.; Rosati, O.; Marini, F.; Fonseca, S. F.; Abenante, L.; Alves, D.; Dabrowska, A.; Kula-Pacurar, A.; Ortega-Alarcon, D.; Jimenez-Alesanco, A.; Ceballos-Laita, L.; Vega, S.; Rizzuti, B.; Abian, O.; Lenardão, E. J.; Velazquez-Campoy, A.; Pyrc, K.; Sancineto, L.; Santi, C. Seleno-Functionalization of Quercetin Improves the Non-Covalent Inhibition of M(pro) and Its Antiviral Activity in Cells against SARS-CoV-2. *Int. J. Mol. Sci.* **2021**, *22*, 7048.
(32) Zhu, H.; Zhang, Y.; Ye, G.; Li, Z.; Zhou, P.; Huang, C. In vivo and *in vitro* antiviral activities of calycosin-7-O-beta-D-glucopyranoside against coxsackie virus B3. *Biol. Pharm. Bull.* **2009**, *32*, 68−73.
(33) Gong, G.; Zheng, Y.; Yang, Y.; Sui, Y.; Wen, Z. Pharmaceutical Values of Calycosin: One Type of Flavonoid Isolated from Astragalus. *Evid. Based Complement. Alternat. Med.* **2021**, *2021*, No. 9952578.

https://doi.org/10.1021/acsomega.2c07259
ACS Omega 2023, 8, 6679−6688

(34) Daina, A.; Michielin, O.; Zoete, V. SwissADME: a free web tool to evaluate pharmacokinetics, drug-likeness and medicinal chemistry friendliness of small molecules. *Sci. Rep.* **2017**, *7*, 42717.
(35) Banerjee, P.; Eckert, A. O.; Schrey, A. K.; Preissner, R. ProTox-II: a webserver for the prediction of toxicity of chemicals. *Nucleic Acids Res.* **2018**, *46*, W257−W263.
(36) Chen, Y. C. Beware of docking! *Trends Pharmacol. Sci.* **2015**, *36*, 78−95.
(37) Sun, D.; Gao, W.; Hu, H.; Zhou, S. Why 90% of clinical drug development fails and how to improve it? *Acta Pharm. Sin. B* **2022**, *12*, 3049−3062.

https://doi.org/10.1021/acsomega.2c07259
ACS Omega 2023, 8, 6679−6688